Shock Waves in an Augmented One-Dimensional Atom Chain

Gabriel STOLTZ
CERMICS, Ecole Nationale des Ponts et Chaussées, 77455 Marne-la-Vallée, France
and
CEA/DAM Ile-de-France, BP 12, 91680 Bruyères-le-Châtel, France
stoltz@cermics.enpc.fr

September 28th, 2004

Abstract

We derive here a simplified discrete one-dimensional (1D) model describing the main features of shock waves. In order to avoid expensive multidimensional simulations, 1D models are commonly used, but the existing ones often exhibit some spurious physically irrelevant behavior. Here we build a 1D model with perturbations arising from mean higher-dimensional behavior. The coupling of the system with a deterministic heat bath "à la" Kac-Zwanzig allows us to derive a generalized Langevin equation for the system, without *a priori* fixing the temperature in the shocked region. This deterministic problem with several degrees of freedom is then reduced to a simpler stochastic problem with memory. Some numerical results are provided, that illustrate and confirm the qualitative correctness of the model.

1 Introduction

The aim of this study is to derive and assess the validity of a simplified microscopic model of shock waves that could help to calibrate parameters for macroscopic descriptions. Shock waves are intrinsically propagative phenomena. It is thus reasonable to describe them within a 1D macroscopic theory. In some cases depending on the geometry, this approximation has proven to be correct [2].

A 1D lattice seems an appropriate model that could, in addition, allow for some mathematical treatment and thus a better theoretical understanding of the phenomena and mechanisms at play. Indeed, many mathematical results are known about the behavior of waves in 1D lattices, concerning the existence of localized waves [10, 22], the form of those waves in the high-energy limit [8] or in the low-energy limit [9], or the behavior under shock [6]. There also exist extended results for a particular interaction between sites, the Toda potential [23] : the structure of a 1D shock is then precisely known, at least in some regime [24].

We begin in section 2 with some introduction to 1D lattice motion, and briefly report on some theoretical results and numerical experiments on piston-impacted shocks. It is shown that, in the absence of a specific treatment, the shock profiles generated significantly differ from shock waves. Especially, their thicknesses grow linearly with time [16, 24], there is no usual equilibration downstream the shock front [3, 18, 24], and relaxation waves do not behave as expected. Indeed, one would expect the shock wave to be a self-similar jump separating two domains at local thermal equilibrium at different temperatures. The relaxation waves should

then catch up the shock front and weaken the shock wave until it disappears. So, we have to introduce higher-dimensional effects, at least in an averaged way. This is performed in section 3. The connection of the chain with a heat bath consisting of a large number of harmonic oscillators, seems to be a good remedy for spurious 1D effects. The shocks generated have constant thicknesses and relaxation waves appear to be properly modelled. We eventually present some simulation results in section 4.

2 The pure 1D model

2.1 Description of the lattice model

We consider a one-dimensional chain of particles with nonlinear nearest-neighbor interactions, described by a potential V. Initially, the particles are at rest at positions $X_n(0) = nd$, which is an equilibrium state for the system. All the masses are set to 1. The normalized displacement of the n-th particle from its equilibrium position is $x_n(t) = \frac{1}{d}(X_n(t) - X_n(0))$. We consider the following normalization conditions [16]:

$$V(0) = 0, \quad V'(0) = 0, \quad V''(0) = 1 \ . \tag{1}$$

The first condition is more a shift on the energy reference, the second one expresses the fact that $x = 0$ is the equilibrium position, and the last one amounts to a rescaling of time. The so-called "reduced relative displacement" is defined as $\delta x_n(t) = x_{n+1}(t) - x_n(t)$.

The Hamiltonian of the system is:

$$H_S(\{x_n\}) = \sum_{n=-\infty}^{\infty} V(x_{n+1} - x_n) + \frac{1}{2}\dot{x}_n^2 \ . \tag{2}$$

The Newton equations of motion read:

$$\ddot{x}_n = V'(x_{n+1} - x_n) - V'(x_n - x_{n-1}) \ . \tag{3}$$

The potential taken here can either have a physical origin, like the 1D Lennard-Jones potential:

$$V_{\mathrm{LJ}}(x) = \frac{1}{8}\left(\frac{1}{(1+x)^4} - \frac{2}{(1+x)^2}\right) \quad , \tag{4}$$

or more mathematical motivations, like the one-parameter Toda potential [23]:

$$V^b_{\mathrm{Toda}}(x) = \frac{1}{b^2}\left(e^{-bx} - 1 + bx\right) \quad . \tag{5}$$

We define $b = -V'''(0)$. The parameter b measures at the first order the anharmonicity of the system. For the Lennard-Jones potential $b = 9$, and for the Toda potential, the parameter b introduced in the definition (5) is indeed equal to $-\dfrac{d^3V^b}{dx^3}(0)$.

2.2 Shock waves in the 1D lattice

2.2.1 A brief review of the existing mathematical and numerical results

A shock can be generated using a "piston" : the first particle is considered as being of infinite mass and constantly moving at velocity u_p. We refer to [4] for a pioneering study of those

shocks in 1D lattices, to [15, 16, 18] for careful numerical experiments and formal analysis, and to [24] for a rigorous mathematical study in the Toda case. All of these studies identify the parameter $a = bu_p$ as critical. When $a < 2$ (note that we use $b = 2\alpha$ with the notation of [16]), the velocity of the downstream particles converge to the piston velocity, in analogy with the behavior of a harmonic lattice (see Figure 1). When $a > 2$, the particles behind the shock experience an oscillatory motion (see Figure 2 to 4). This behavior is quite similar to what is happening in hard-rod fluids (see [18] for a more precise description of that phenomenon), and has to be linked to the exchange of momenta happening when two particles collide in a 1D setting. This was also noticed for other potentials such as the Lennard-Jones potential, and can be used to define specific 1D thermodynamical averages [3].

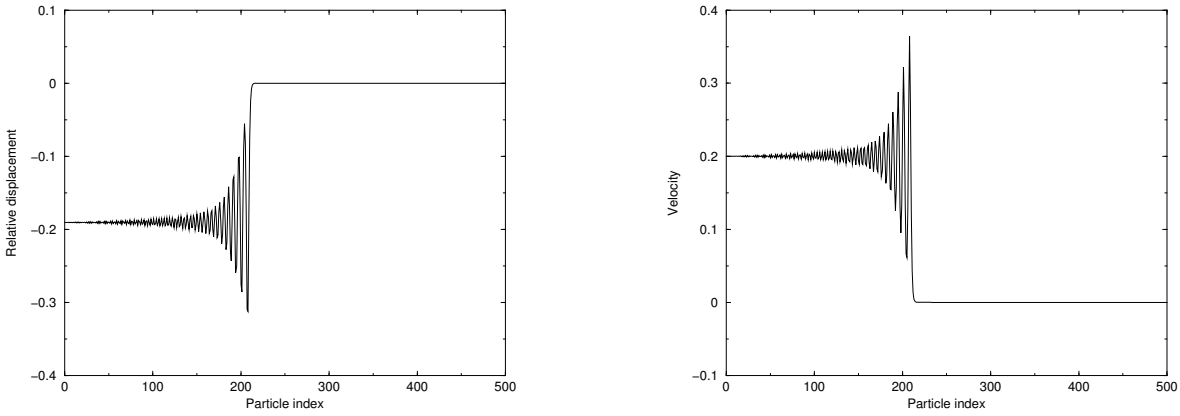

Figure 1: Relative displacement (left) and velocity profiles (right) versus particle index for a weak shock at a representative time: number of particles $N_{\text{part}} = 500$, Toda parameter $b = 1$, piston velocity $u_p = 0.2$ so that $a = 0.2$. The particle are taken initially at rest at their equilibrium positions.

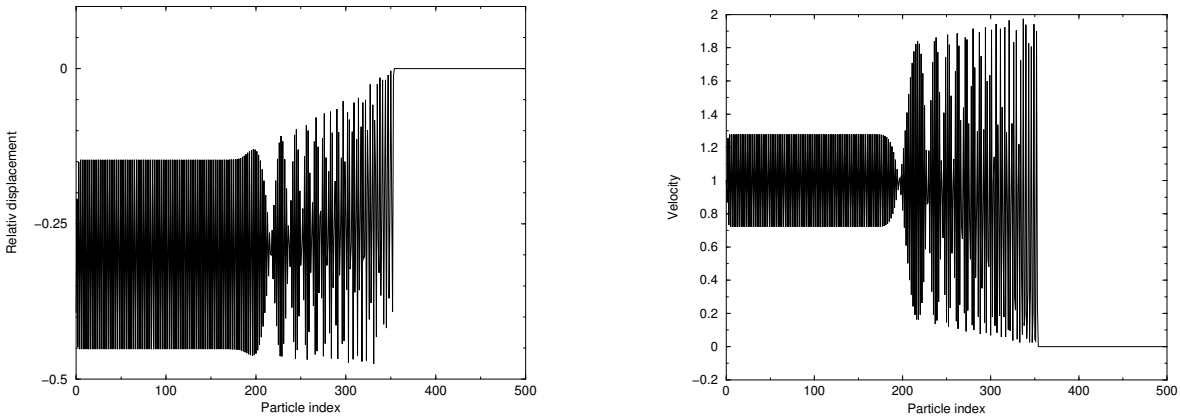

Figure 2: Relative displacement (left) and velocity profiles (right) versus particle index for a strong shock at time $T = 100$: $b = 10$, $u_p = 1$ so that $a = 10$. The particles are initially at rest.

In the case of a strong shock ($a > 2$) and in the Toda case, the displacement pattern is particularly well understood from a mathematical point of view [24]: the lattice can be decomposed in three regions. In the first one, for $n > N_{\max}t$, the particles have "almost"

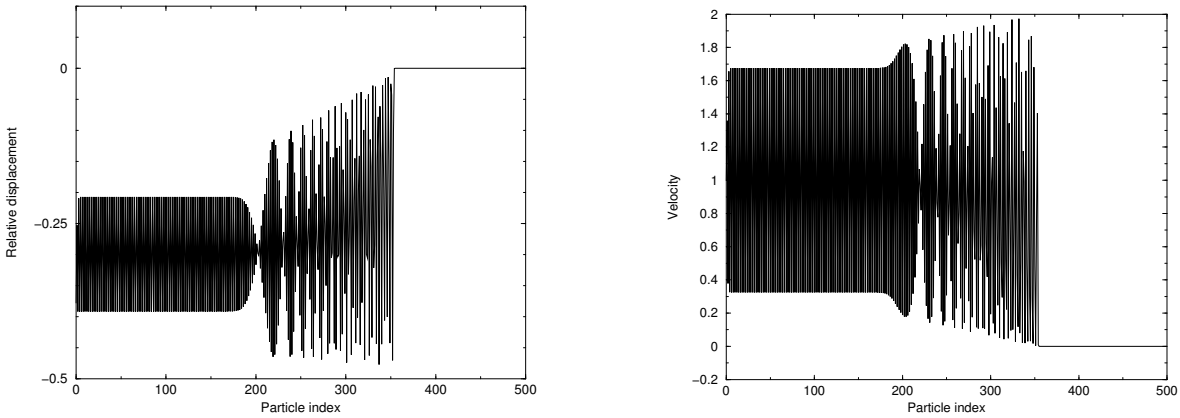

Figure 3: Relative displacement (left) and velocity profiles (right) versus particle position for a strong shock at time $T = 100.12$ using the same conditions as for Figure 2. Notice how the downstream quantities changed.

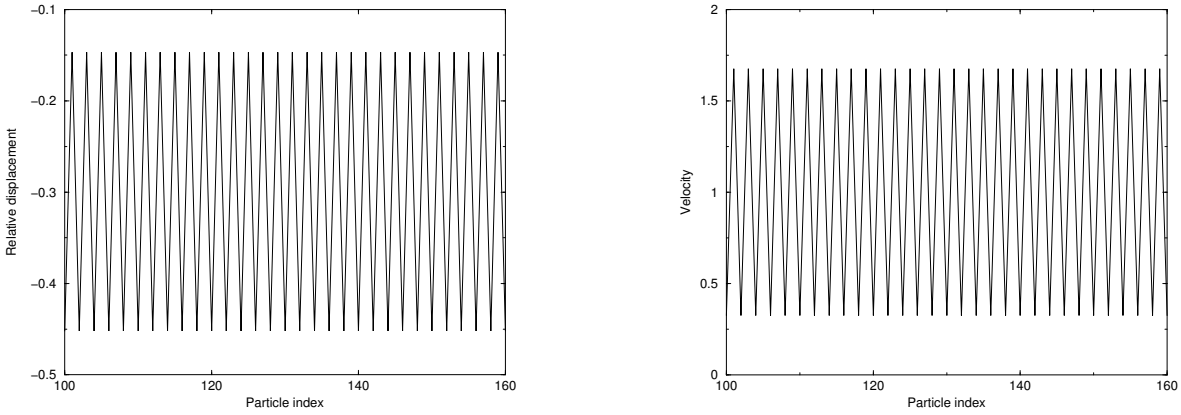

Figure 4: Left: Zoom on the relative displacement pattern of Figure 2. Right: Zoom on the velocity pattern of Figure 3. Notice the oscillatory distribution for the downstream quantities.

not felt the shock yet, and their displacements are exponentially small. The second region, whose thickness grows linearly in time ($N_{\min}t < n < N_{\max}t$), is composed of a train of solitons. We recall that solitons are particular solutions of the Toda lattice model, and correspond to localized waves [23]. In the third region ($n < N_{\min}t$), the lattice motion converges to an oscillatory pattern of period 2 (binary wave). The motion behind the shock is asymptotically described by the evolution of a single oscillator (see [3] for a precise description of this behavior). There is no local thermal equilibrium in the usual sense (*i.e.* the distribution of the velocities is not of Boltzmann form). This was already mentioned in [18].

2.2.2 Density plots.

To get a better understanding of the shock patterns, it is convenient to represent the system in terms of local density. This local density can be obtained as a function of the local average of the interatomic distances, both in space and time. We restrict ourselves to a local average in space.

More precisely, the local averaged interatomic distance of the n-th length is denoted by $\overline{\delta x_n}$, and given by:

$$\overline{\delta x_n} = \sum_{i=-\infty}^{+\infty} \alpha_j \ \delta x_{n+j} \ .$$

The local density ρ_n is then defined as:

$$\rho_n = \left(1 + \overline{\delta x_n}\right)^{-1} \ .$$

The weights $\{\alpha_j\}$ are chosen in practice to be non negative and of sum equal to one. A convenient choice is for example:

$$\alpha_j = C^{-1} \cos\left(\frac{j}{2M+1}\pi\right)$$

for $-M \leq j \leq M$, and $\alpha_j = 0$ otherwise. C is a normalization factor:

$$C = \sum_{j=-M}^{M} \cos\left(\frac{j}{2M+1}\pi\right) \ .$$

The integer M is the local range of averaging.

Figure 5 gives the densities corresponding to the relative displacement patterns of figures 1 and 2.

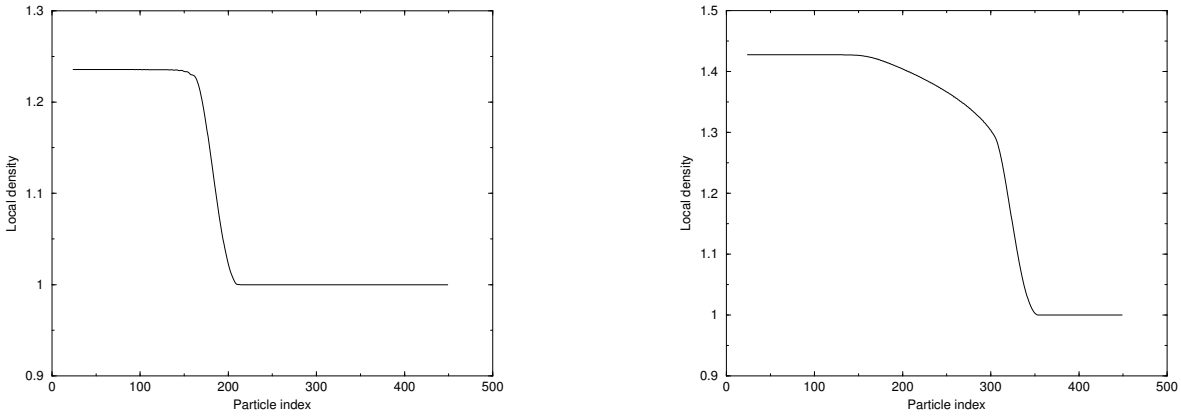

Figure 5: Density patterns for the relative displacement pattern of the weak shock of Figure 1 (left) and the strong shock of Figure 2 (right). The local averaging range is $M = 50$.

2.2.3 Simulation of piston compression

We first implement a preliminary thermalization. The particles are taken initially at rest at their equilibrium positions. We then randomly draw displacements x_n and velocities $\dot{x}_n$ according to the probability density

$$d\nu = \bigotimes_{n=-\infty}^{\infty} Z^{-1} e^{-\frac{1}{2}\beta_x(x_n^2+\dot{x}_n^2)} \ dx_n d\dot{x}_n \ , \tag{6}$$

Z^{-1} being a normalization factor. The initial displacements and velocities are then of order $\frac{1}{\sqrt{\beta_x}}$. Notice that we take small initial displacements, so we approximate the full potential $V(x)$ by its harmonic part $\frac{1}{2}x^2$. This approximation is of course justified at the beginning of the simulation, when displacements are small enough. After this initial perturbation, we let the system free to evolve during a typical time $T_{\text{init}} = 10$. The simulations were performed using a Velocity Verlet scheme, the time step being chosen to have a relative energy conservation $\frac{\Delta E}{E}$ of about 10^{-5}.

At time T_{init} the piston impact begins: the first particle is kept moving toward the right at constant velocity u_p.

We emphasize that the shock patterns are robust, in the sense that they remain essentially unchanged when initial thermal pertubations are supplied. This point was already noted in [18] where the authors gave numerical evidence of that fact. While rigorously proven only in the Toda lattice case for a lattice initially at rest at equilibrium, the above shock description seems then to remain qualitatively valid for a quite general class of potentials and with random initial conditions. We make a comparison of the different profiles in Figures 6 to 8: the patterns on the left are those of a shock using thermal initial conditions, the patterns on the right are those of a lattice initially at rest at equilibrium. The profiles are indeed quite conserved, especially the density profiles.

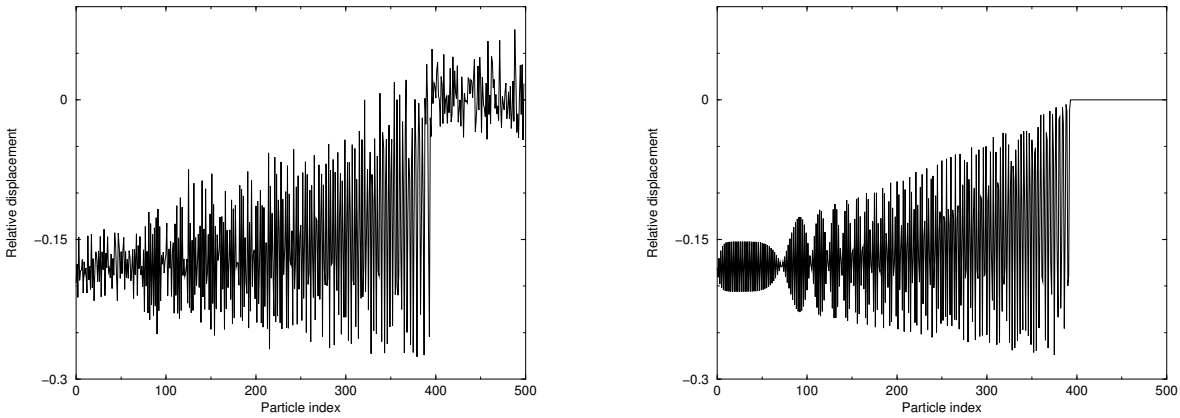

Figure 6: Relative displacement profiles for a thermalized strong shock using a Toda potential with $b = 10$, and comparison with the reference profile corresponding to a lattice initially at rest. The piston speed is $u_p = 0.3$ so that $a = 3$, $\frac{1}{\sqrt{\beta_x}} = 0.02$.

For strong shocks ($a > 2$), the shock front thickens linearly with time as can be seen in Figure 9. This is in contradiction with what is observed in shock propagation experiments as well as in 3D numerical simulations. Moreover the velocity distribution behind the shock front shows that the downstream particles experience a (quasi-)oscillatory motion in the range $[0, 2u_p]$. This is of course not the case for 3D simulations, where the particle velocities are much less correlated, and appears to be a pure 1D effect.

We emphasize once again that initial thermal perturbations are not sufficient to remedy these spurious 1D effects since the patterns obtained in Figures 6 to 8 are very similar. In the sequel we are going to build a 1D model that enables us to get rid of these undesired effects.

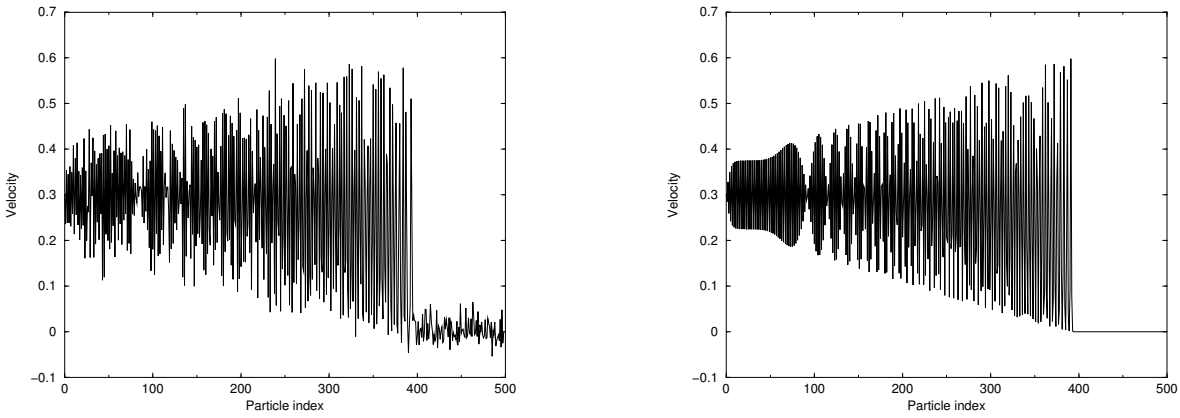

Figure 7: Velocity profiles for the same conditions as for Figure 6

.

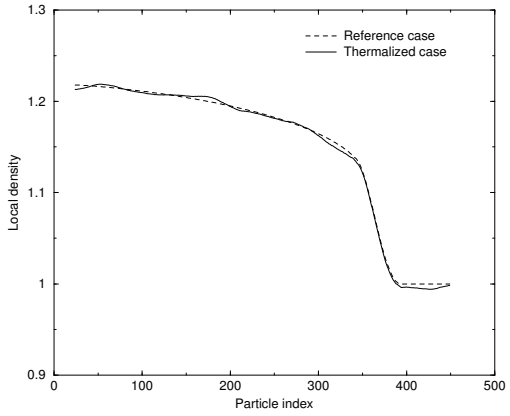

Figure 8: Local density profiles corresponding to Figure 6 with $M = 50$. Dashed line: reference profile. Solid line: Thermalized profile. Notice that both patterns almost coincide.

2.2.4 Simulation of relaxation waves

In order to study the relaxation waves, the piston is removed after a compression time t_0, and the systems evolves freely during time $t_1 - t_0$.

The results are once again not physically satisfactory. The soliton train of Figure 10, which was less visible in Figure 6, is not destroyed by the relaxation waves. It travels on and widens since the solitons move away from each others (the distance between the fastest ones, that is, the more energetic ones, and the slowest ones, increases). This kind of dispersion can be seen in Figure 11. A zoom of the end of the soliton train is shown in Figure 12. We emphasize that the energy remains localized in those waves, so there is no damping of these solitons. Rarefaction is only observed in the region behind the soliton train.

On the other hand, in 3D simulations or in experiments, one observes a progressive damping of the whole compressive wave. This is a second spurious effect of the 1D model we would like to get rid of and that our model will able to deal with.

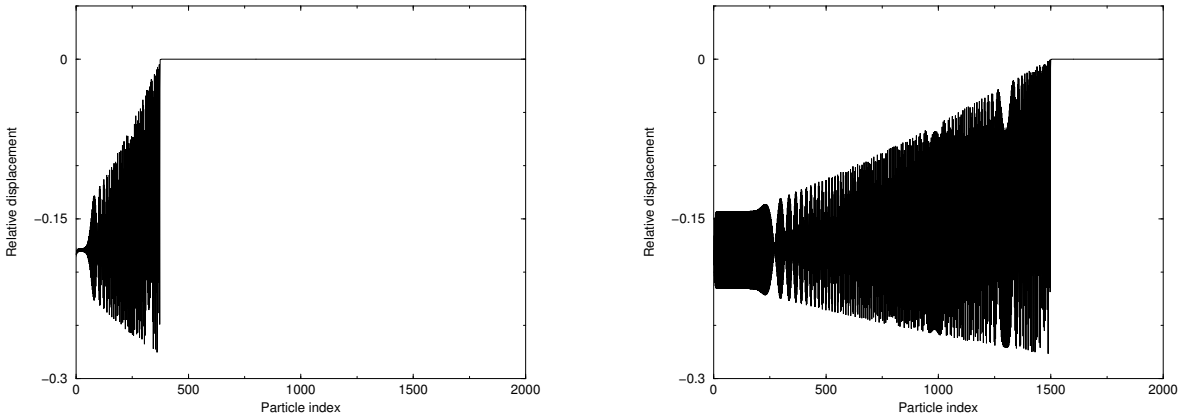

Figure 9: Relative displacement patterns for the same conditions as in Figure 6 (reference case). Left: Snapshot at time $T_1 = 200$. The shock front corresponds (roughly) to the zone between particle $n_{\min} = 60$ and particle $n_{\max} = 350$. Right: Snapshot at time $T_2 = 800$. The shock front corresponds to the zone between particle number $n_{\min} = 250$ and particle number $n_{\max} = 1500$. Thus the shock front is indeed growing linearly in time.

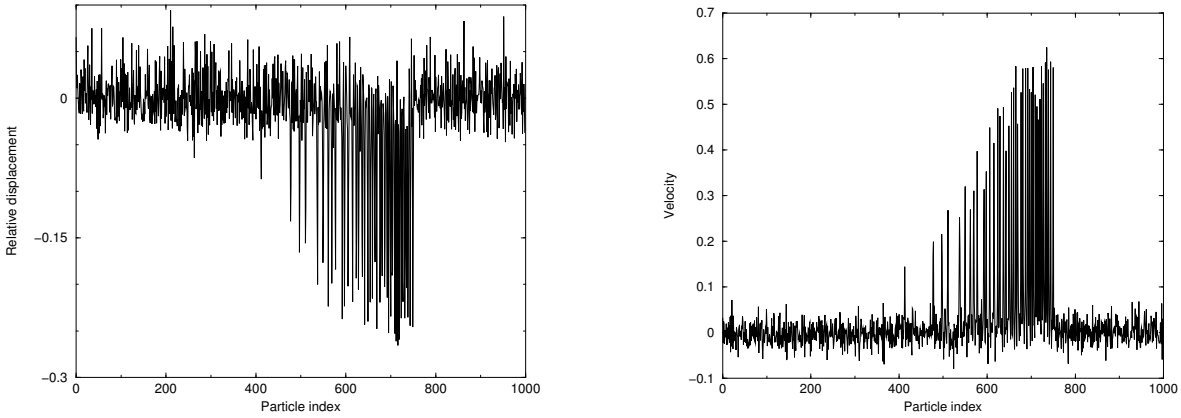

Figure 10: Relative displacement and speed profiles for the same parameters as in figure 6. The compression time is now $t_0 = 50$, and the relaxation time is $t_1 - t_0 = 350$.

3 Introduction of mean higher-dimensional effects

The results of the previous section indicate the need for a modeling of perturbations arising from the transverse degrees of freedom existing in higher dimensional simulations. Such perturbations will interfere with the soliton train at the front, and possibly damp it. Perturbations in the longitudinal direction, such as thermal initialization for the x_n, cannot do this, as shown by Figures 6 to 8.

Actually, some facts are already known about the influence of 3D effects for shock waves. In [14, 17] Holian *and al.* pointed out the fact that even a 1D shock considered in 3D (that is to say, a piston compression along a principal direction of a crystal for example) may not look like the typical 1D pattern of Figures 1 or 2. If the crystal is at zero temperature, then the compression pattern in 3D is the same as the 1D one, with a soliton train at the front. But if positive temperature effects are considered, the interactions of the particles with their

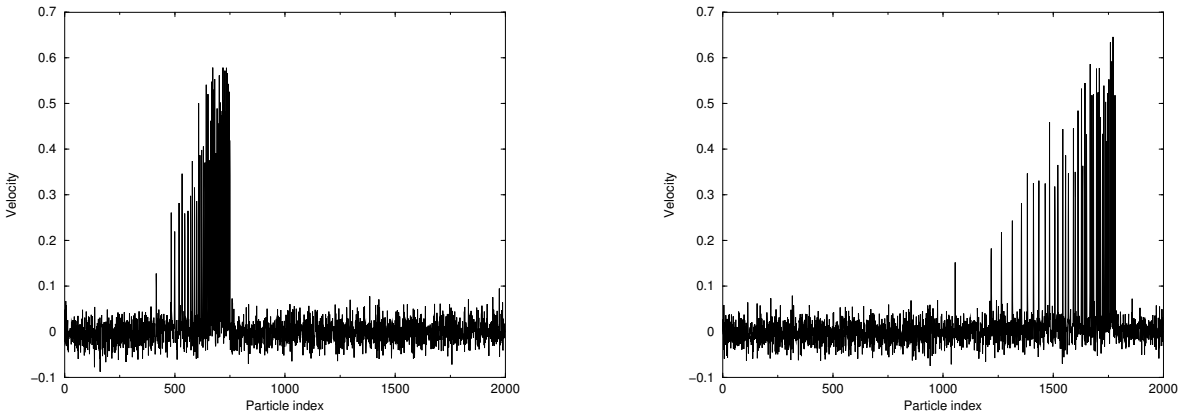

Figure 11: Behavior of the soliton train in time. Left: Velocity profile for the same parameters as in figure 10. Right: Same parameters except higher relaxation time $t_1 - t_0 = 900$. Notice that the solitons remain unchanged, but there is dispersion within the soliton train, since the the solitons do not have the same velocities.

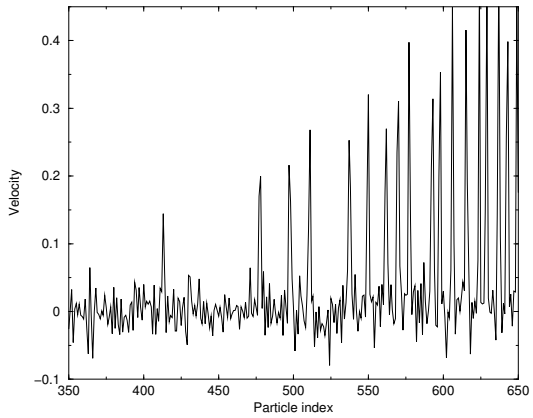

Figure 12: Zoom of the end of the soliton train of Figure 10 - Right. The solitons are localized waves moving on and are unaffected by the relaxation of the downstream domain.

neighbors - especially in the transverse directions - lead to the destruction of the coherent soliton train at the front, and a steady-regime can be reached (shock with constant thickness).

To the best of the author's knowledge, there is no existing model that could both account for these higher dimensional effects and be mathematically tractable. We introduce a classical heat bath model, as an idealized way to couple the longitudinal modes of the atom chain to other modes. This model is justified to some extent by heuristic considerations in section 3.1. We are then able to derive a generalized Langevin equation describing the evolution of the system.

3.1 Form of the perturbations arising from higher dimensional degrees of freedom

Consider the system described in Figure 13. We still consider a 1D atom chain, but each particle in the 1D chain also interacts with two particles outside the horizontal line. These

particles are supposed to mimic some effects of transverse degrees of freedom. The transverse particles are placed in the middle of the springs and have only one degree of freedom, namely their ordinates y_n. The particles in the 1D chain are still supposed to have only one degree of freedom as well. This means that we constrain them to remain on the horizontal line. The interactions between the particles in the chain and the particles outside the chain are ruled by a pairwise interaction potential, for example the same potential as for interactions in the 1D chain.

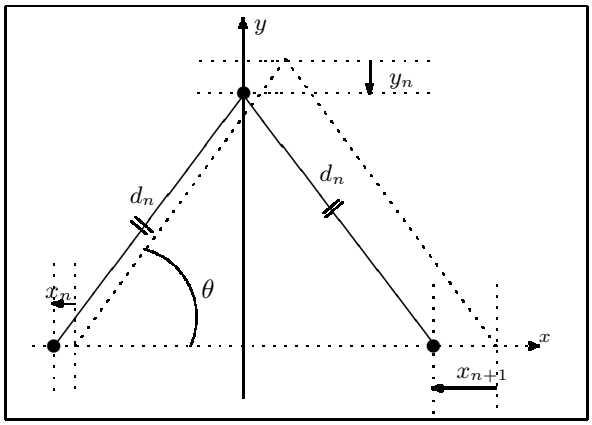

Figure 13: Notations for the interaction of a transverse particle with particles on the 1D atom chain.

We consider small displacements around equilibrium positions. All the computations are done at first order in the displacements x_n, y_n. Therefore, we can consider the pairwise interaction potentials to be of harmonic type. Up to a normalization, and for a displacement x from equilibrium position, $V(x) = \frac{1}{2}x^2$.

We first turn to the case $\theta = \frac{\pi}{3}$ corresponding to a 2D regular lattice. At first order,

$$d_n = \left[\left(\frac{1}{2}(1 + x_{n+1} - x_n)\right)^2 + \left(\frac{\sqrt{3}}{2} + y_n\right)^2\right]^{1/2} = 1 + \frac{1}{2}(x_{n+1} - x_n) + \frac{\sqrt{3}}{2}y_n \ .$$

We now focus on the evolution of x_n. Considering only interactions with the neighboring particles on the horizontal line, and the additional interaction with the particle y_n,

$$\ddot{x}_n = \frac{5}{4}(x_{n+1} - 2x_n + x_{n-1}) + \frac{\sqrt{3}}{2}(y_n - y_{n-1}) \ .$$

The equation governing the evolution of y_n is:

$$\ddot{y}_n = -\frac{3}{2}y_n - \frac{\sqrt{3}}{2}(x_{n+1} - x_n) \ .$$

More generally, consider the system of Figure 13 with a general angle θ. The equilibrium distance is now $d^0 = \frac{1}{2\cos\theta}$, and the corresponding normalized harmonic potential is $V(d) = \frac{1}{2}(\frac{d}{d^0} - 1)^2$.

The normalized distance $\bar{d}_n = \dfrac{d_n}{d^0}$ is now

$$\bar{d}_n = 1 + 2\cos^2\theta(x_{n+1} - x_n) + 2\sin\theta\cos\theta \cdot y_n \ .$$

The additional longitudinal force exerted on x_n by y_n is then

$$f_n = 2\cos^2\theta\left[\cos\theta(x_{n+1} - x_n) + \sin\theta \cdot y_n\right] \ .$$

Summing over N particles that do not interact with each other, each one being characterized by an angle θ_i, the additional force on x_n is seen to be of the form

$$F_n = A_N(x_{n+1} - 2x_n + x_{n-1}) + \sum_{i=1}^{N} K_i(y_n^i - y_{n-1}^i) \ ,$$

with $K_i = 2\cos^2\theta_i \sin\theta_i$ and $A_N = \sum_{i=1}^{N} 2\cos^3\theta_i$. So, the equation of motion for x_n is

$$\ddot{x}_n = (1 + A_N)(x_{n+1} - 2x_n + x_{n-1}) + \sum_{i}^{N} K_i(y_n^i - y_{n-1}^i) \ . \tag{7}$$

The equations for the y_n^i can be obtained in the same way as before:

$$\ddot{y}_n^i = -a_i y_n^i - K_i(x_{n+1} - x_n) \ . \tag{8}$$

These linear perturbations are only valid for small displacements, *i.e.* when the approximation of the full potential by its harmonic part is justified. Notice moreover that we discard any type of interaction of the y particles with each others.

However, this motivates an attempt to take into account missing degrees of freedom by introducing a heat bath whose form will lead to equation of motion similar to (7) - (8). We now turn to this task.

3.2 Description of the heat bath model

We consider the following Hamiltonian for a coupled system consisting of the system under study (S) and a heat bath (B) described by bath variables $\{y_n^j\}$ ($n \in \mathbb{Z},\ j = 1, \ldots, N$). To use a heat bath is classical but was never done in the context of 1D chains to the author's knowledge.

The full Hamiltonian reads:

$$H(\{x_n,\ y_n^j\}) = H_S(\{x_n\}) + H_{SB}(\{x_n,\ y_n^j\}) \tag{9}$$

where H_S is given by (2), and

$$H_{SB}(\{x_n,\ y_n^j\}) = \sum_{n=-\infty}^{\infty} \sum_{j=1}^{N} \frac{1}{2} m_j (\dot{y}_n^j)^2 + \frac{1}{2} k_j \left(\gamma_j(x_{n+1} - x_n) - y_n^j\right)^2 \tag{10}$$

The interpretation is as follows: We consider each spring length $\delta x_n = x_{n+1} - x_n$ as thermostated by a heat bath $\{y_n^j\}$, in the spirit of [7, 25]. The parameter k_j is the spring constant of the j-th oscillator, m_j its mass, γ_j weights the coupling between Δx_n and y_n^j. Note

that although more general cases can be considered [19, 21], the coupling is taken bilinear in the variables, for it allows for an exact mathematical treatment. Indeed, a generalized Langevin equation (GLE) can be easily recovered (see [7, 25] for seminal examples). To our knowledge, it is also the only case where the limit $N \to \infty$ can be rigorously justified.

Other physical motivations may be presented, such as the representation of extra variables in Fourier modes leading to a Hamiltonian similar to (9), see [1]. These extra degrees of freedom allow for some "transverse" radiation of the energy.

3.3 Derivation of the generalized Langevin equation

3.3.1 General procedure

Up to a rescaling of y_n^j, we may assume that all masses m_j are 1. The only parameters left for the coupling are the coupling factors γ_j.

We also introduce the pulsations ω_j given by:

$$\omega_j = \left(\frac{k_j}{m_j}\right)^{1/2} = k_j^{1/2} \ .$$

The equations of motion read:

$$\ddot{x}_n = g_N(x_{n+1} - x_n) - g_N(x_n - x_{n-1}) - \sum_{j=1}^{N} \gamma_j \omega_j^2 (y_n^j - y_{n-1}^j) \ , \tag{11}$$

$$\ddot{y}_n^j = -\omega_j^2 \left(y_n^j - \gamma_j (x_{n+1} - x_n)\right) \ , \tag{12}$$

where

$$g_N(x) = V'(x) + \left(\sum_{j=1}^{N} \gamma_j^2 \omega_j^2\right) x \ . \tag{13}$$

Notice the strucutral similarities of (11) with (7) and of (12) with (8).

The procedure is classical [25]: We integrate (12) for $\{y_n^j\}$ and then insert the solutions in (11) for $\{x_n\}$. The integrability of the system is clear (once initial conditions in velocities and displacements are set) when the force g_N is globally Lipschitz. This is for example the case when the sum $\sum_{j=1}^{N} \gamma_j^2 \omega_j^2$ is finite, and when V' is globally Lipschitz, which is indeed true for the Toda potential (5). For the Lennard-Jones potential (4) it remains true as long as the energy of the system is finite (since the potential diverges when $x \to -1$, the bound on the total energy implies $x > x_0 > -1$, and a bound on the Lipschitz constant can be given by $V'(x_0)$).

The computation gives:

$$y_n^j(t) = y_n^j(0)\cos(\omega_j t) + \frac{\dot{y}_n^j(0)}{\omega_j}\sin(\omega_j t) + \int_0^t \gamma_j \omega_j \sin(\omega_j s)(x_{n+1} - x_n)(t-s)\ ds \ .$$

Integrating by parts and inserting in (11):

$$\begin{aligned} \ddot{x}_n(t) = {} & V'(x_{n+1} - x_n) - V'(x_n - x_{n-1}) \\ & + \int_0^t K_N(s)(\dot{x}_{n+1} - 2\dot{x}_n + \dot{x}_{n-1})(t-s)\ ds + r_n^N(t) \ , \end{aligned} \tag{14}$$

where

$$K_N(t) = \sum_{j=1}^{N} \gamma_j^2 \omega_j^2 \cos(\omega_j t) \quad ,$$

$$r_n^N(t) = -\sum_{j=1}^{N} (y_n^j(0) - y_{n-1}^j(0))\gamma_j\omega_j^2 \cos(\omega_j t) + (\dot{y}_n^j(0) - \dot{y}_{n-1}^j(0))\gamma_j\omega_j^2 \frac{\sin(\omega_j t)}{\omega_j} \quad . \\ -\gamma_j^2 k_j \cos(\omega_j t)(x_{n+1} - 2x_n + x_{n-1})(0)$$

Formally, (14) looks like a GLE, provided r_n^N is a random forcing term. The dissipation term involves a memory kernel K_N and an "inner" friction $\dot{x}_{n+1} - 2\dot{x}_n + \dot{x}_{n-1}$ (which is a discrete quantity analogous to the second viscosity in hydrodynamics [13]). So, we are left with a description of the system only in terms of $\{x_n\}$. To further specify the terms, we have to describe the choice of the heat bath spectrum $\{\omega_j\}$, the coupling constant γ_j and the initial conditions for the bath variables.

3.3.2 Choice of the constants

We choose the values:

$$\omega_j = \Omega \left(\frac{j}{N}\right)^k, \quad \gamma_j^2\omega_j^2 = \lambda^2 f^2(\omega_j)\ (\Delta\omega)_j \ , \quad f^2(\omega) = \frac{2\alpha}{\pi}\frac{1}{\alpha^2 + \omega^2} \tag{15}$$

where $(\Delta\omega)_j = \omega_{j+1} - \omega_j$, $\alpha, \lambda > 0$ and $k > 0$.

The function f^2 is defined this way for reasons that will be made clear in section 3.4. The heat bath spectrum $\{\omega_j\}$ is more dense as N increases. The exponent k accounts for the repartition of the pulsations. More general choices could be made, involving randomly sampled pulsations [20]. However, we restrict ourselves to the case of deterministic pulsations.

We emphasize here once again that the constants chosen and the form of the coupling are not new. A similar choice is made in [20]. The novelty is in the application to a 1D chain, that is, we consider independent heat baths, each heat bath corresponding to a spring length.

We now motivate (15). Notice that we impose an upper bound to the heat bath spectrum: this is related to the discreteness of the medium. Indeed, for a system at rest with particles distant from 1, the higher pulsation allowed is π, corresponding to an oscillatory motion of spatial period 2. When particles come closer (for example if the mean distance between particles is $a < 1$), the higher pulsation increases to the value $\frac{\pi}{a}$ since the lowest spatial period is now $2a$. Taking then lower bound d_m for the minimal distance between neighbouing particles, we get an upper bound for the spectrum, namely $\Omega = \frac{\pi}{d_m}$.

The choice of the coupling constants between the system and the bath is an important issue. The only purpose of the heat bath in a 1D shock simulation is to mimic some effects of dimensionality, such as energy transfer to the tranverse modes. This energy transfer can be quantified using (12). Indeed, the total energy transfer for a harmonic oscillator of pulsation ω subjected to an external forcing σ is known [1]. More precisely, consider the following harmonic oscillator:

$$\ddot{z} + \omega^2 z = h(t) \ , \tag{16}$$

where h is an external time-dependent forcing term. Then the total energy transfered by the external forcing to the system (from $t = -\infty$ to $t = +\infty$ for a system at rest at $t = -\infty$) is

$\Delta E = \frac{1}{2}|\hat{h}(\omega)|^2$. The energy transfer to the heat bath occurs as described by (12). This gives a total energy transfer for a spring $x_{n+1} - x_n$ considered initially at rest:

$$\Delta E_n = \frac{1}{2}\sum_{j=1}^{N} \gamma_j^2 \omega_j^4 |\widehat{\Delta x_n}(\omega_j)|^2 \ . \tag{17}$$

As a first approximation, a shock profile can be described as a self-similar jump: $\Delta x_n(t) = \delta H(t - n\tau)$, where $\delta < 0$ is the jump amplitude, τ the shock speed, and H is the Heaviside function. Then, $|\widehat{\Delta x_n}(\omega)| = \omega^{-1}$. The energy transfer (17) is then

$$\Delta E_n = \frac{1}{2}\sum_{j=1}^{N} \gamma_j^2 \omega_j^2 \ .$$

With the spectrum (15), the condition $\Delta E_n \to C$ with $0 < C < \infty$ is satisfied:

$$\Delta E_n = \frac{\lambda^2}{2}\sum_{j=1}^{N} f^2(\omega_j)(\Delta\omega)_j \to \frac{\lambda^2}{2}\int_0^{\Omega} f^2 = \lambda^2 \sigma(\Omega) \ .$$

The last expression is bounded since f^2 is integrable (We recall $\displaystyle\int_0^{\infty} f^2 = 1$). σ is a C^∞ function. Notice that the above convergence results from the convergence of the Riemann sum appearing on the left.

3.3.3 Choice of the initial conditions.

We consider initial conditions $\{y_n^j(0),\ \dot{y}_n^j(0)\}$ randomly drawn from a Gibbs distribution with inverse temperature $2\beta_y$. This distribution is conditioned by the intial data $\{x_n,\ \dot{x}_n\}$. The quadratic nature of the Hamiltonian (9) shows that the Gibbs measure is Gaussian. More precisely, we set

$$y_n^j(0) = \gamma_j(x_{n+1} - x_n)(0) + \left(\frac{1}{2\beta_y k_j}\right)^{1/2} \chi_j^n \tag{18}$$

$$\dot{y}_n^j(0) = \left(\frac{1}{2\beta_y}\right)^{1/2} \mu_j^n \tag{19}$$

where $\chi_j^n, \mu_j^n \sim \mathcal{N}(0,1)$ are independent sequences of standard Gaussian.

With these choices,

$$r_n^N(t) = \frac{1}{\sqrt{2\beta_y}}\sum_{j=1}^{N} \omega_j\gamma_j \cos(\omega_j t)(\chi_n^j - \chi_{n-1}^j) + \omega_j\gamma_j \sin(\omega_j t)(\mu_n^j - \mu_{n-1}^j) \ . \tag{20}$$

The probability space is induced by the mutually independent sequences of independently and identically distributed (i.i.d.) random variables $\chi_n^j,\ \mu_n^j$. In fact, the random variables $\chi_n^j - \chi_{n-1}^j$ and $\mu_n^j - \mu_{n-1}^j$ are also independent Gaussian random variables (with respect to the index j), with mean 0 and variance 2. We denote them $\sqrt{2}\xi_n^j,\ \sqrt{2}\eta_n^j$. So,

$$r_n^N(t) = \frac{\lambda}{\sqrt{\beta_y}}\sum_{j=1}^{N} f(\omega_j)\cos(\omega_j t)\xi_n^j + f(\omega_j)\sin(\omega_j t)\eta_n^j\ (\Delta\omega)_j^{1/2} \ .$$

For fixed N, the above expressions give

$$\mathbb{E}(r_n^N(t)r_n^N(s)) = \frac{1}{\beta_y}K_N(t-s)\ . \tag{21}$$

This relation is known as the fluctuation-dissipation relation, linking the random forcing term and the memory kernel. The behavior of the system when $N \to \infty$ is then an interesting issue, that can help us to get a better understanding of the phenomenas at play.

3.4 Limit when $N \to \infty$

3.4.1 Limit of the dissipation term

The memory kernel can be seen as a Riemann sum. The limit is then:

$$K_N(t) = \lambda^2 \sum_{j=1}^{N} f^2(\omega_j)\cos(\omega_j t)(\Delta\omega)_j \to \lambda^2 \int_0^\Omega f^2(\omega)\cos(\omega t)\ dt =: \lambda^2 K_\Omega(t) \tag{22}$$

when $N \to \infty$, the convergence holding in $L^1[0,T]$, $T > 0$.

The special choice (15) implies $K_\Omega(t) \to e^{-\alpha t}$ when $\Omega \to \infty$ in the norm of continuous functions. The memory kernel is then exponentially decreasing.

3.4.2 Limit of the fluctuation term

The limit $N \to \infty$ gives the convergence in a weak sense in $C[0,T]$ (see the Appendix and [20]) toward a stochastic integral (Wiener integral):

$$r_n^N(t) \to \lambda r_n^\Omega(t) := \frac{\lambda}{\sqrt{\beta_y}} \int_0^\Omega f(\omega)\cos(\omega t)dW_\omega^{n,1} + f(\omega)\sin(\omega t)dW_\omega^{n,2} \tag{23}$$

where $W_\omega^{n,1}, W_\omega^{n,2}$ $(n \in \mathbb{Z})$ are independent standard Brownian motions.

3.4.3 Limit of the equation

Formally, we obtain in the limit $N \to \infty$ a stochastic integro-differential equation (IDE):

$$\boxed{\begin{aligned} \ddot{x}_n(t) &= V'(x_{n+1}-x_n) - V'(x_n - x_{n-1}) \\ &\quad +\lambda^2 \int_0^t K_\Omega(s)(\dot{x}_{n+1} - 2\dot{x}_n + \dot{x}_{n-1})(t-s)\ ds + \frac{\lambda}{\sqrt{\beta_y}} r_n^\Omega(t)\ \ , \end{aligned}} \tag{24}$$

with

$$K_\Omega(t) = \int_0^\Omega f^2(\omega)\cos(\omega t)d\omega \xrightarrow[\Omega\to\infty]{} e^{-\alpha t}\ \ ,$$

$$r_n^\Omega(t) = \int_0^\Omega f(\omega)\cos(\omega t)dW_\omega^{n,1} + f(\omega)\sin(\omega t)dW_\omega^{n,2}\ \ ,$$

and the fluctuation-dissipation relation

$$\mathbb{E}(r_n^\Omega(t)r_n^\Omega(s)) = \frac{1}{\beta_y}K_\Omega(t-s)\ . \tag{25}$$

The random process r_n^Ω is the stationary Gaussian process with zero mean and autocovariance function K_Ω. It is in fact an Ornstein-Uhlenbeck process.

The way the solutions of (14) converge to the solutions of (24) can be made rigorous by a direct adaptation of the results of [20]: the convergence of x_n^N solution of (14) to x_n solution of (24) is weak in $C^2[0,T]$ (in the sense of continuous random processes). We refer to the Appendix for some precisions on the proof.

The limiting equation (23) shows the main effects of the heat-bath interaction: The pure 1D equation (3) is supplemented by two terms, one dissipation term with an exponentially decreasing memory, and a random forcing. Therefore the heat bath acts first as an energy trap, absorbing some of the energy of the shock when it passes. This energy is then given back to the system through the random forcing term to an amount precised by (25). This allows the equilibration of the downstream domain. This heuristic interpretation is confirmed by some numerical simulations of (14) in section 4.

3.5 Generalization of the system-bath interaction

The Hamiltonian of the system can be written in an abstract form as

$$H(x,\ y_N) = \frac{1}{2}|\dot{x}|^2 + F(x) + \frac{1}{2}|M\dot{y_N}|^2 + \frac{1}{2}|Ax - By_N|^2 \tag{26}$$

where $x = (\ldots, x_{n-1}, x_n, x_{n+1}, \ldots)$ and $y_N = (\ldots, y_{n-1}^1, \ldots, y_{n-1}^N, y_n^1, \ldots, y_n^N, \ldots)$. The matrix M is a mass matrix (operator), A and B are general operators, $F(x) = \sum_{n=-\infty}^{\infty} V(x_{n+1} - x_n)$.

In the previous example, B was diagonal. But more generally, B could be considered as tridiagonal: this could model the interaction of two neighboring heat baths linked to neighboring spring lengths.

4 Numerical results

We integrate the equations of motion (11), (12) for a given N. The system is initialized with velocities and displacements that are randomly sampled, using (18) and (19) in the y-coordinates, and (6) in the x coordinates. Note that the quantities $\dfrac{1}{\beta_x}$ and $\dfrac{1}{\beta_y}$ may differ. The system is then first let to evolve freely, so that the coupling between transverse and longitudinal directions starts.

Shock waves are generated using a piston in the same fashion as in 2.2.3, giving Figures 14 to 16. We then study relaxation waves (Figures 20 to 21).

The time-step Δt is chosen to ensure a relative energy conservation of 10^{-5}. Typically, $\Delta t = 0.01$. The spectrum density parameter k in (15) is taken to be $k = 1$. Other choices lead to the same kind of simulation results.

Notice that, if L represents the size of the 1D chain, the algorithmic complexity scales as $O(LN)$. The computations were made on an usual desktop computer (Pentium 1.0 GHz), and only took about a couple of hours for the most demanding ones.

4.1 Sustained shock waves

Figures 14 to 19 show the different patterns obtained in the case of a system coupled to a heat bath. The profiles of the thermalized shock of Figures 6 to 8 are reproduced on the right

of each figure for the sake of comparison.

Notice that the upper bound to the spectrum, Ω, is of order π since the shock is not too strong, and hence the medium is not too compressed. The parameter α is taken less or equal to Ω so that K_Ω and $\sigma(\Omega)$ are sufficiently close from their limiting values. The parameter λ is fitted numerically to obtain sharp profiles. If λ is too small, the coupling is too weak and the profiles look like the pure 1D ones. If λ is too high, the forcing may be too strong, leading to the collapse of two neighboring particles. A good choice of λ involves a good rate of energy transfer to the transverse modes.

The results show that the introduction of transverse degrees of freedom has important consequences on the pure 1D pattern. The soliton train at the front is destroyed, and the shock thickness is constant along time, and indeed as sharp as possible in view of the value of λ, instead of growing in time as in the pure 1D case.

This is to the author's knowledge the first result of this kind for a 1D chain. Thus a steady regime can now be reached, and these simulations really seem to deserve the name "shock waves". In contrast to the pure 1D model results, these simulations have now the same qualitative behavior as 3D simulations or experiments.

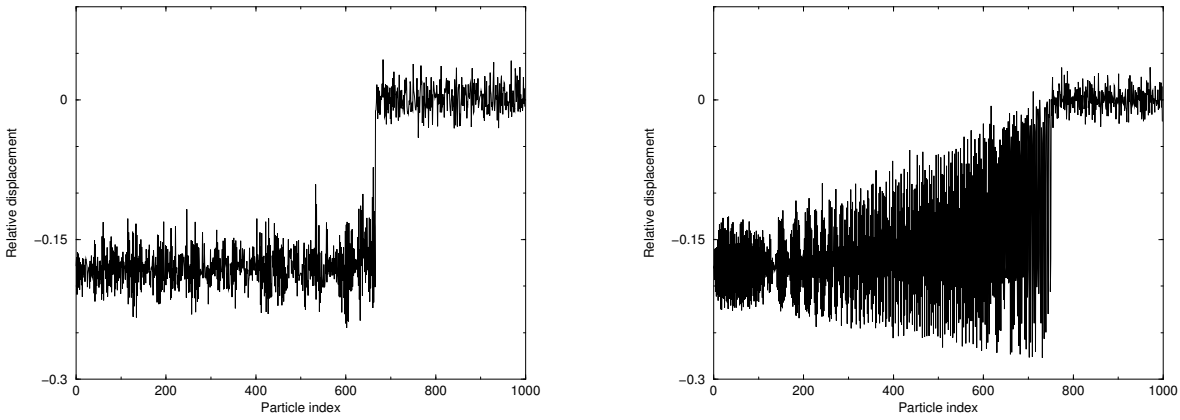

Figure 14: Relative displacement profiles for the system coupled to a heat bath (left), and comparison with a thermalized shock (right). For the thermalized shock, the parameters are $u_p = 0.3$, $b = 10$ and $\frac{1}{\sqrt{\beta_x}} = 0.01$. For the system coupled to a heat bath, the additional parameters are $\frac{1}{\sqrt{\beta_y}} = 0.02$, $\alpha = 5$, $\Omega = 10$, $\lambda = 0.5$. The number of transverse oscillators is $N = 25$.

4.2 Rarefaction waves

As can be seen in Figures 20 and 21, a rarefaction wave develops and progressively weakens the shock (notice that the velocities decrease and that the relative displacement increase compared to Figures 14 to 16). This is indeed the expected physical behavior for a viscous fluid. This dissipation can be interpreted as energy transfer to the transverse modes.

Besides, no soliton train survives, contrarily to the pure 1D case, where the solitons are not destroyed and move on unperturbed. In the pure 1D case, there is no weakening of the initial wave, only dispersion. Once again, to our knowledge, this is the first time a 1D discrete model behaves as expected.

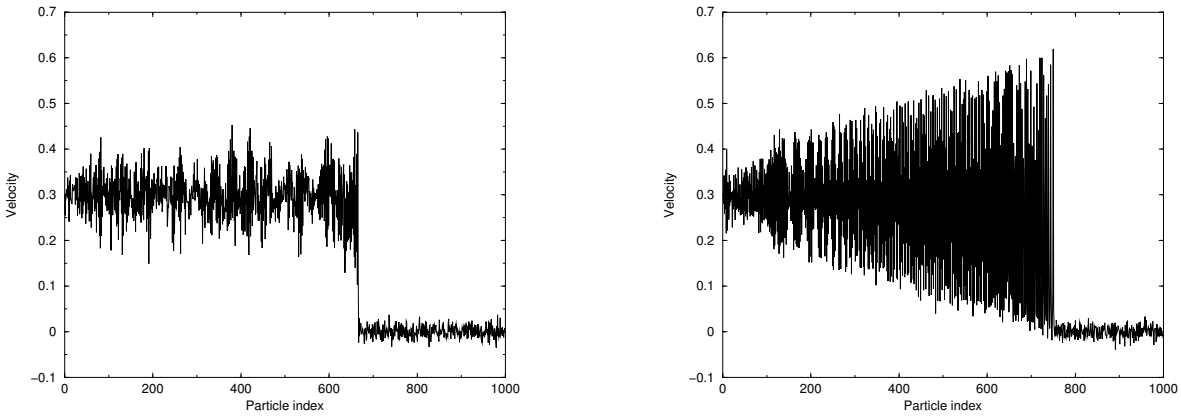

Figure 15: Velocity profiles for the same simulations as in Figure 14.

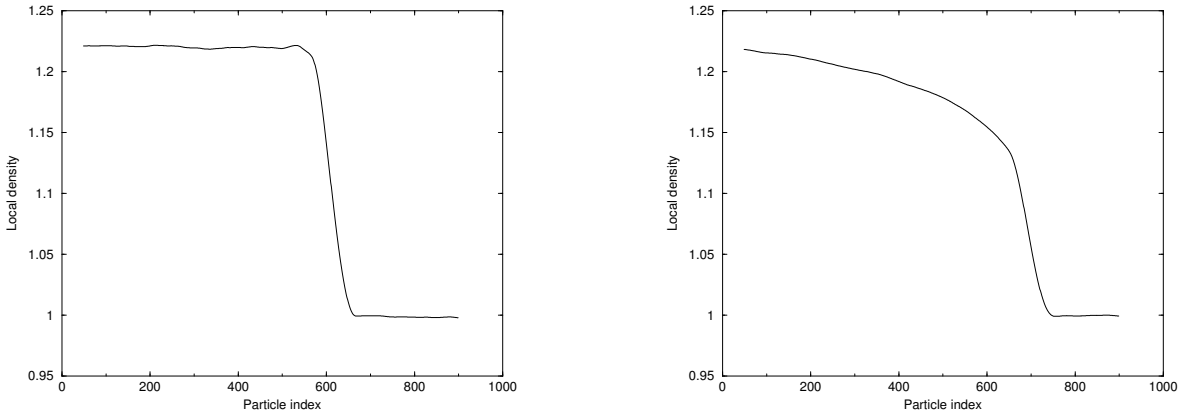

Figure 16: Local density profiles for the same simulations as in Figure 14.

5 Conclusion

This study indicates a possible track to thermostate a 1D lattice in a deterministic way, without fixing the temperature as would require a Langevin simulation. Indeed, when the shock passes, the temperature changes, and a Langevin simulation asks for an *a priori* knowledge of the temperature in the shocked region.

The interactions of the chain and the bath naturally lead to memory effects, and can be described by a memory kernel, at least in some limiting regime. Numerical experiments illustrate the success of this method.

This model indeed qualitatively reproduces the most important features of shock waves (sharpness of the shock front, existence of relaxation waves, equilibration after the shock has passed). This is in contrast with the classical pure 1D model.

However, this heat-bath thermalization is better suited for shocks that are not too strong. On the other hand, for strong shocks, nonlinear effects should play an important role in the energy transfer in the transverse modes, and a bilinear coupling such as (10) may not be a relevant modelling. In this case, a nonlinear coupling in the spirit of [19] should be more adapted.

An interesting issue is now to compare those reduced 1D profiles with profiles arising from

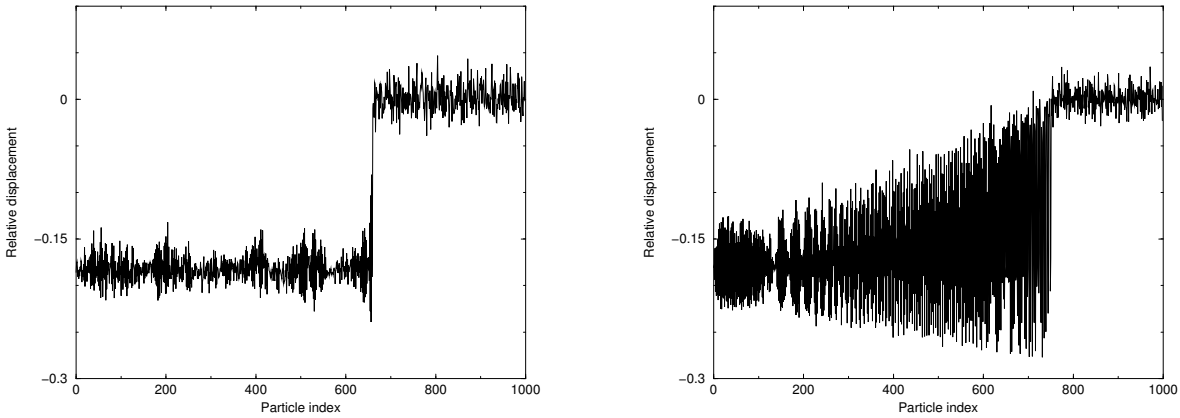

Figure 17: Same parameters as for Figure 14, except for the system coupled to a heat bath, $N = 100$.

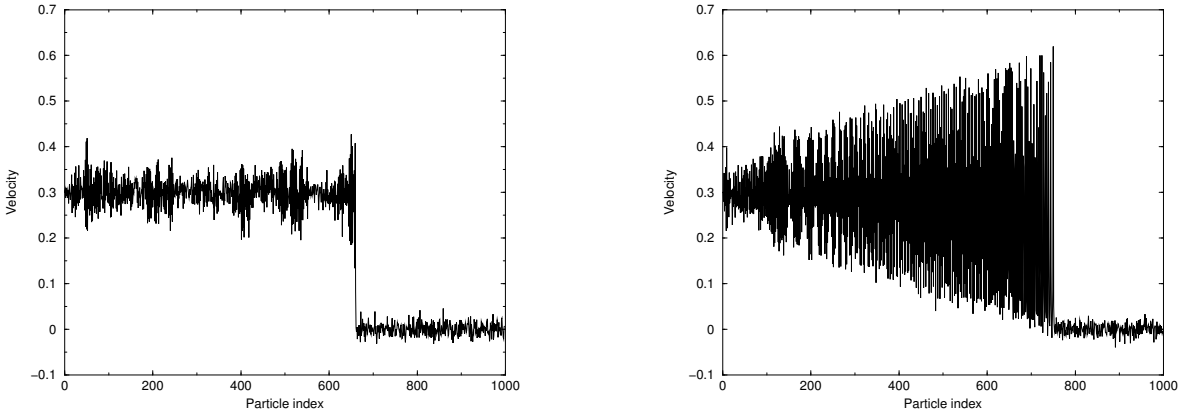

Figure 18: Velocity profiles for the same simulations as in Figure 14.

full 3D simulations, and to precise the comparison in a more quantitative way.

Acknowlegements.

I thank Claude Le Bris and Eric Cancès (CERMICS) for constant support and careful re-reading of the manuscript, and Laurent Soulard (CEA/DAM) for helpful discussions about the physics of shock waves. I also express special thanks to Andrew Stuart (University of Warwick) for very fruitful discussions on heat-bath models and related topics.

References

[1] L. Bruneau and Stephan De Bivre. A Hamiltonian model for linear friction in a homogeneous medium. *Comm. Math. Phys.*, 109:511–542, 2002.

[2] R. Courant and K.O. Friedrichs. *Supersonic flow and shock waves.* Springer, 1991.

[3] W. Dreyer and M. Kunik. Cold, thermal and oscilator closure of the atomic chain. *J. Phys. A*, 33(10):2097–2129, 2000.

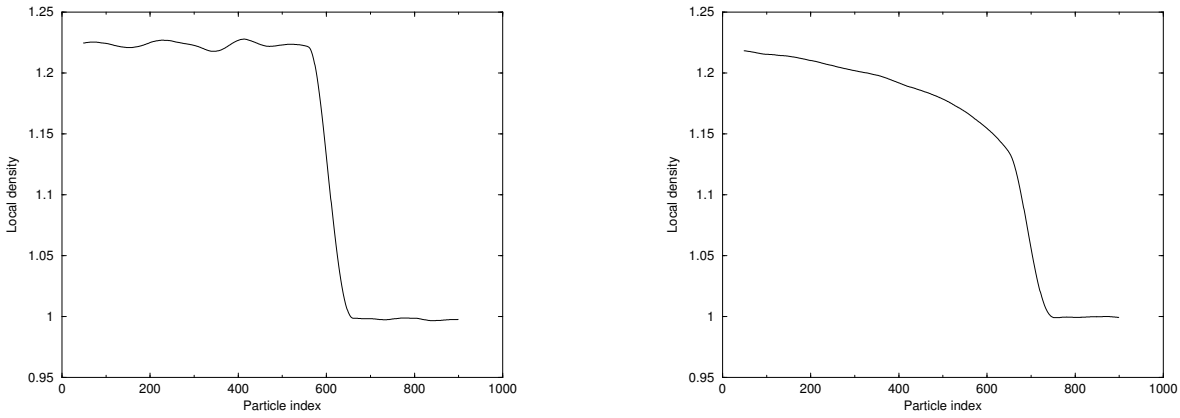

Figure 19: Local density profiles for the same simulations as in Figure 14.

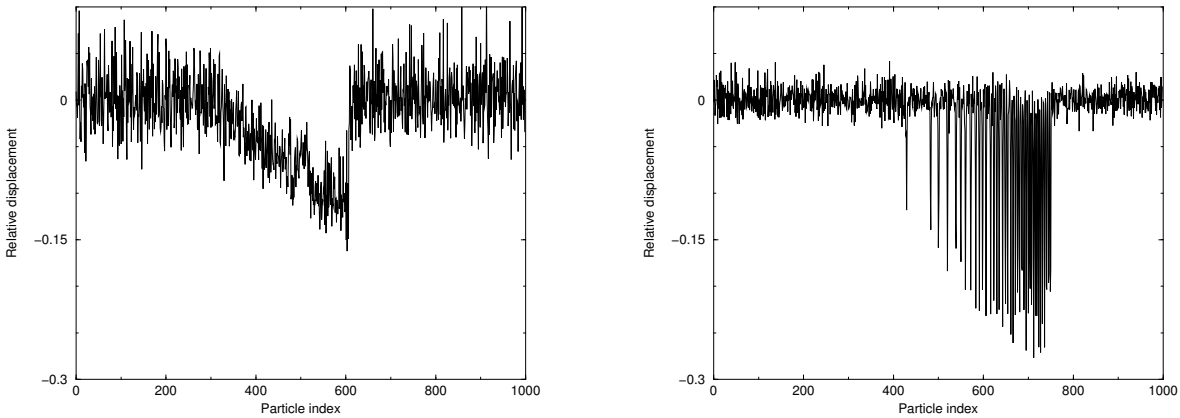

Figure 20: Relative displacement profiles for the system coupled to a heat bath (left) and the thermalized 1D system (right). The parameters for the system coupled to a heat bath are $\frac{1}{\sqrt{\beta_y}} = 0.04$, $\alpha = 2$, $\Omega = 5$, $\lambda = 0.5$. The system is compressed during $t_0 = 50$. The relaxation time is $t_1 - t_0 = 350$.

[4] G.E. Duvall, R. Manvi, and S.C. Lowell. Steady shock profile in a one-dimensional lattice. *J. Appl. Phys.*, 40(9), 1969.

[5] W. Fickett and W.C. Davis. *Detonation*. Dover Publication Inc., 2000.

[6] A.-M. Filip and S. Venakides. Existence and modulation of traveling waves in particle chains. *Comm. Pure Appl. Math.*, 52:693–735, 1999.

[7] G.W. Ford, M. Kac, and P. Mazur. Statistical mechanics of assemblies of coupled oscillators. *J. Math. Phys.*, 6:504–515, 1965.

[8] G. Friesecke and K. Matthies. Atomic scale localization of high energy solitary waves on lattices. *Physica D*, 171:211–220, 2002.

[9] G. Friesecke and R.L. Pego. Solitary waves on lattices: I. Qualitative properties, renormalization and continuum limit. *Nonlinearity*, 12:1601–1627, 1999.

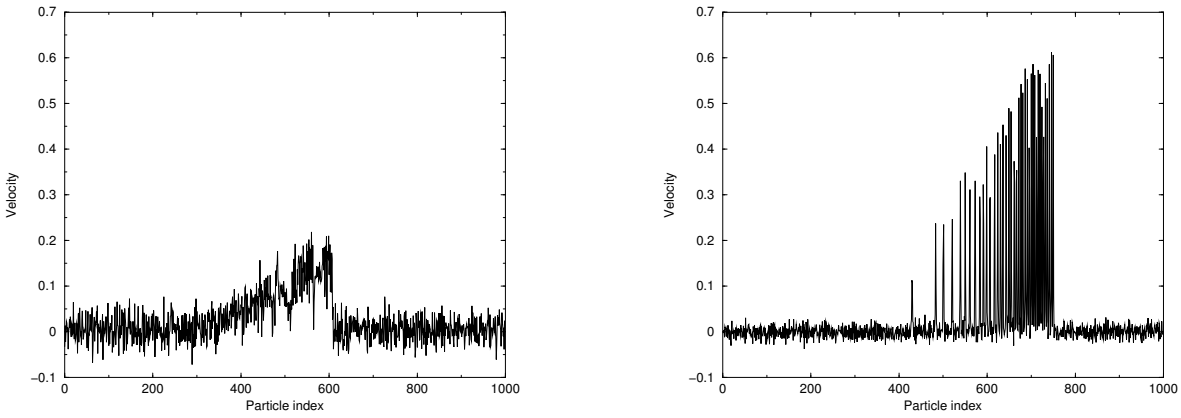

Figure 21: Velocity profiles for the same simulations as in Figure 20.

[10] G. Friesecke and J. Wattis. Existence theorem for solitary waves on lattices. *Comm. Math. Phys.*, 161:391–418, 1994.

[11] I.I. Gikhman and A.V. Skorokhod. *The theory of stochastic processes*. Springer, 2004.

[12] O.H. Hald and R. Kupferman. Asymptotic and numerical analyses for mechanical models of heat baths. *J. Stat. Phys.*, 106:1121–1184, 2002.

[13] J. Hietarinta, T. Kuusela, and B. Malomed. Shock waves in the dissipative Toda lattice. *J. Phys. A*, 28:3015–3024, 1995.

[14] B.L. Holian. Atomistic computer simulations of shock waves. *Shock Waves*, 5:149–157, 1995.

[15] B.L. Holian, H. Flaschka, and D.W. McLaughlin. Shock waves in the Toda lattice: Analysis. *Phys. Rev. A*, 24 (5):2595–2623, 1981.

[16] B.L. Holian and G.K. Straub. Molecular dynamics of shock waves in one-dimensional chains. *Phys. Rev. B*, 18(4):1593–1608, 1978.

[17] B.L. Holian and G.K. Straub. Molecular dynamics of shock waves in three dimensional solids. *Phys. Rev. Lett.*, 43:1598, 1979.

[18] B.L. Holian, G.K. Straub, and R.G Petscheck. Molecular dynamics of shock waves in one-dimensional chains. II. Thermalization. *Phys. Rev. B*, 19(8):4049–4055, 1979.

[19] R. Kupferman and A.M. Stuart. Fitting SDE models to nonlinear Kac-Zwanzig heat bath models. *Physica D (in press)*, 2003.

[20] R. Kupferman, A.M. Stuart, J.R. Terry, and P.F. Tupper. Long-term behaviour of large mechanical systems with random initial data. *Stochastics and Dynamics*, 2(4):1–30, 2002.

[21] K. Lindenberg and V. Seshadri. Dissipative contributions of internal multiplicative noise. I. Mechanical oscilator. *Physica A*, 109:483–499, 1981.

[22] D. Smets and M. Willem. Solitary waves with prescribed speed on infinite lattices. *Journal of Functional Analysis*, 149:266–275, 1997.

[23] M. Toda. *Theory of Nonlinear Lattices*. Springer, 1981.

[24] S. Venakides, P. Deift, and R. Oba. The Toda shock problem. *Comm. Pure Appl. Math.*, 14:1171–1242, 1991.

[25] R. Zwanzig. Nonlinear generalized Langevin equations. *J. Stat. Phys.*, 9:215–220, 1973.

Appendix

The proof of the convergence of the solutions of (14) to the solutions of (24) can be done as in [20]. We have to extend it here to the multi-dimensional case in order to deal with convergence of sequences.

We note x_n^N the solution of (14) for a given number N of transverse variables. We set $\delta x_n^N = x_{n+1}^N - x_n^N$. The solution of (24) is noted x_n. We set $\lambda = 1$ to simplify notations. The extension to more general values of λ is straightforward.

The space of real sequences in noted $\mathcal{H} = \mathbb{R}^{\mathbb{N}}$, and is equiped with the usual l^∞-norm. For a sequence $z = \{z_n\} \in \mathcal{H}$:

$$|z|_{l^\infty} = \sup_{n\in\mathbb{Z}} |z_n| \ .$$

The space $\mathcal{H}$ endowed with this norm is then a separable complete metric space.

Consider the array of spring lenghts

$$Q_N = \begin{pmatrix} \vdots \\ \delta x_n^N \\ \vdots \end{pmatrix}$$

and the array of random forcing terms

$$G_N = \frac{1}{\beta_y} \begin{pmatrix} \vdots \\ r_n^N \\ \vdots \end{pmatrix} \ .$$

We similarly define Q and G for the sequence $\{x_n\}$.

The linear operator A, acting on sequences $z = \{z_n\} \in \mathcal{H}$, is defined by $Az = \{Az_n\} = \{z_{n+1} - 2z_n + z_{n-1}\}$. It follows $|Az|_{l^\infty} \leq 4|z|_{l^\infty}$.

Equation (14) can be rewritten as (recall $\lambda = 1$)

$$\ddot{Q}_N = AF(Q_N) + \int_0^t K_N(s) A\dot{Q}_N(t-s)\ ds + G_N(t) \ .$$

Introducing $\mathcal{K}_N(t) = \int_0^t K_N(s)\ ds$ and integrating the convolution term by parts, (14) becomes

$$\ddot{Q}_N - \left(AF(Q_N) + \int_0^t \mathcal{K}_N(s) A\ddot{Q}_N(t-s)\ ds \right) = G_N(t) - A\dot{Q}_N(0)\mathcal{K}_N(t) \ . \tag{27}$$

This equation can be rewritten under a fixed point form as

$$(Id + R_N)\ddot{Q}_N(t) = F_N(t) \ . \tag{28}$$

As F is Lipschitz, $||R_N||$ is small for small T. An usual Picard argument gives the existence and uniqueness of $\ddot{Q}_N \in C([0,T],\mathcal{H})$ solving (28) for T small enough (see [12], section 12, for an analogous proof). Standard results also give the continuity of $\ddot{Q}_N$ on $\mathcal{K}_N \in L^1[0,T]$ and $U_N = G_N - AQ_N(0)\mathcal{K}_N \in C([0,T],\mathcal{H})$. The mapping $(K_N, U_N) \mapsto Q_N$ is then continuous from $L^1[0,T] \times C([0,T],\mathcal{H})$ to $C([0,T],\mathcal{H})$ with the corresponding norms.

The convergence of K_N in $L^1[0,T]$ is straightforward, and implies the convergence of $\mathcal{K}_N$ in $L^1[0,T]$.

The convergence of U_N results from the convergence of $\mathcal{K}_N \in L^1[0,T]$ and from the convergence of G_N to G (in a way to precise). We refer to [11], section VI.4., Theorem 2. Considering the collection of continuous real-valued stochastic processes G_N with values in $\mathcal{H}$ (which is a separable complete metric space), we have to show:

1. The finite-dimensional distributions of G_N weakly converge to those of G, which is a continuous process.

2. A tightness inequality of the form

$$\mathbb{E}\left[|G_N(t+u) - G_N(t)|_{l^\infty}^2\right] \leq C|u| \ .$$

Then it follows $G_N \Rightarrow G$ in $C([0,T],\mathcal{H})$-weak.

These two points are straightforward generalizations of the proof in [20] (in the case of non-random pulsations ω_j) when extended to sequences with values in $\mathcal{H}$. Point 1 can be verified since the components of G_N are i.i.d. Gaussian random variables. We then get the convergence $U_N \Rightarrow U$ in $C([0,T],\mathcal{H})$-weak.

The convergences of K_N to K in $L^1[0,T]$ and U_N to U in $C([0,T],\mathcal{H})$ in a weak sense then give the convergence of $\ddot{Q}_N$ in $C([0,T],\mathcal{H})$ in a weak sense. Therefore, $Q_N \Rightarrow Q$ in $C^2([0,T],\mathcal{H})$-weak. This implies the convergence in a weak sense for all the components of Q_N for T small enough.

For general t, consider $e^{-\gamma t}Q_N$ for γ large enough, and rescale appopriately the operators appearing in (28). The proof then follows the same lines.